Comparative Study of Pitting Corrosion in 316L Stainless Steel Using Different Metal Additive Manufacturing Techniques

Tze Yi Leow[1], Kia Wai Liew[2*], Carla Canturri[3], Poh Kiat Ng[4], Aishwarya[5], Robert Shandro[6]

[1,2,4]*Machine Design and Tribology (SIG), Centre for Advanced Mechanical and Green Technology, Faculty of Engineering and Technology, Multimedia University, Jalan Ayer Keroh Lama, 75450 Melaka, Malaysia; *E-mail address of corresponding author: kwliew@mmu.edu.my*

[3,5,6]*Matcor Technology & Services Pte Ltd, 3 Seletar Aerospace Link, 797550, Singapore.*

Abstracts: 316L stainless steel is a commonly used material in a range of industries, including the automotive and aerospace industries, due to its advantageous mechanical properties, such as high yield strength and outstanding corrosion resistance. In recent years, the use of metal additive manufacturing technologies for fabricating 316L stainless steel has become more common, as it permits the creation of intricate geometries that are difficult to achieve through conventional manufacturing techniques. Nevertheless, certain characteristics of additive-manufactured 316L stainless steel, such as its pitting corrosion resistance, remain insufficiently understood. In the present experimental study, a pitting corrosion test was performed in accordance with ASTM G48 standards. The pitting corrosion test was conducted with the use of ferric chloride solution on 316L LPBF, 316L MBJ, and 316L WAAM additive-manufactured stainless steel. The data was compared to wrought 316L stainless steel. The results of the investigation indicate that 316L LPBF exhibited the highest pitting corrosion resistance, followed by 316L WAAM, wrought 316L, and 316L MBJ. Microstructure analysis further demonstrated that grain size played significant roles in the pitting corrosion resistance performance of the materials, with smaller grain size yielding superior performance. Additionally, Vickers hardness testing revealed that specimens with higher hardness exhibited better pitting corrosion resistance.

Keywords: Additive Manufacturing, 316L Stainless Steel, Pitting Corrosion, Microstructure, Hardness.

1. INTRODUCTION

In the context of the transition towards the Fourth Industrial Revolution (4IR), additive manufacturing plays a crucial role as it facilitates the production of intricately designed and customised products [1]. With notable advancements in additive manufacturing technologies and enhanced product quality, its application has extended across various industries, including aerospace [2], biomedical [3], construction [4], and manufacturing [5]. Metal additive manufacturing entails the incremental layer-by-layer fabrication of metallic objects through the selective addition of materials until the entire object is formed [6]. Additive manufacturing is widely employed for rapid prototyping, enabling the fabrication of components with highly intricate geometries that were previously unattainable using conventional manufacturing techniques [7].

Despite the advancements in the metal additive manufacturing industry, there is still a limited understanding of certain aspects, particularly the corrosion resistance of additive-manufactured stainless steels [8], [9]. In the case of traditional manufacturing methods, a higher understanding of the corrosion processes has been attained with the susceptibility to corrosion in stainless steels having been demonstrated in the past [10]. The corrosion rates of stainless steel have been reported to range from 0.05-2 mm/year in concentrated, deaerated alkaline aqueous environments above 60°C, to 18 mm/year in de-aerated 50 wt% NaOH solution at 90°C [10]. Various factors contribute to the corrosion of 316L stainless steel, including exposure to high chloride environments that result in pitting corrosion [11]. Additive-manufactured steels, similar to conventionally manufactured steels, are prone to corrosion-related damages such as pitting corrosion, which can lead to part failure and catastrophic consequences [12], [13]. The critical pitting temperature, which denotes the minimum temperature at which corrosion pits do not form, has significant implications for the service temperature of additive-manufactured stainless steels [9]. Given the potential hazards associated with corrosion effects on additive-manufactured steels, it is imperative to

comprehend the impact of pitting corrosion on additive-manufactured steel produced using different additive manufacturing methods and compare its corrosion resistance to that of conventionally manufactured steels.

Therefore, the current work aims to investigate the pitting corrosion resistance and to determine the critical pitting temperature (CPT) of additive-manufactured 316L stainless steel produced through three different additive manufacturing methods: Laser-Powder Bed Fusion (316L LPBF), Metal Binder Jetting (316L MBJ), and Wire Arc Additive Manufacturing (316L WAAM). The corrosion performance of the additive-manufactured 316L stainless steel samples will be compared to that of 316L stainless steel samples fabricated using the conventional hot rolling manufacturing method (316L Wrought).

2. EXPERIMENTAL WORK

2.1. Specimen Preparation

316L LPBF specimens were produced using an EOS M290 Metal 3D Printer that used a 400-watt fiber laser for the incremental fusion of 316L stainless steel powder. The printing process involved layer-by-layer construction, with a layer height of 40 µm, a focus diameter of 100 µm, and argon gas utilized as the shielding gas. In contrast, 316L MBJ specimens were fabricated using a DMP 2000 Metal Binder Jetting Printer, which used a binder liquid to selectively bind layers of 316L stainless steel powder. Furthermore, 316L WAAM specimens were fabricated through the application of a Gas Metal Arc Welding (GMAW) additive manufacturing machine. This method involved the sequential melting of a 1.2 mm diameter 316L stainless steel wire and its subsequent deposition layer by layer. Notably, the layer thickness of the WAAM specimens is 2.1 mm, with the torch travel speed set at 0.9 m/min and wire feed speed set at 7.5 m/min. Additionally, a maximum interlayer temperature of 150 °C was maintained during the fabrication process. Figure 1 displays the various shapes and sizes of the 316L stainless steel samples produced through different additive manufacturing methods. To standardise the specimens, all samples were cut into dimensions of 15 mm × 15 mm × 5 mm (L × W × H), as depicted in Figure 2. The specimen surface with dimension of 15 mm × 15 mm is the X-Y plane. To ensure consistency of the pitting corrosion test, the surfaces of all specimens underwent grinding to achieve a 1000-grit surface finish, as illustrated in Figure 3(a). For microstructural analysis and hardness testing, the surface finish was further refined to a 1-micron mirror finish, as shown in Figure 3(b).

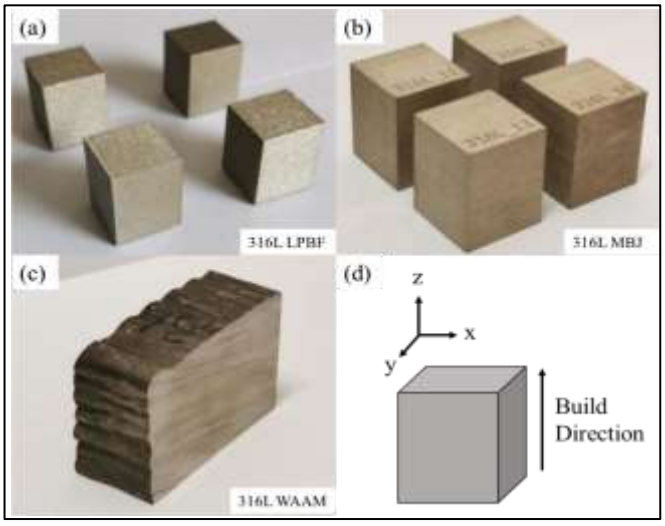

Fig. 1: Additive-manufactured 316L stainless steel samples, (a) 316L LPBF, (b) 316L MBJ, (c) 316L WAAM, and (d) sample build direction

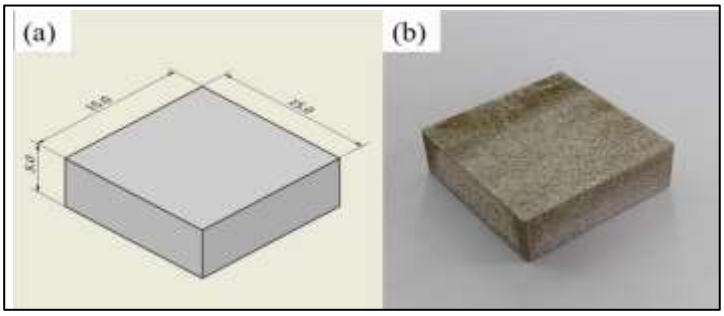

Fig. 2: (a) CAD drawing with dimension in mm and, (b) photograph of test specimen

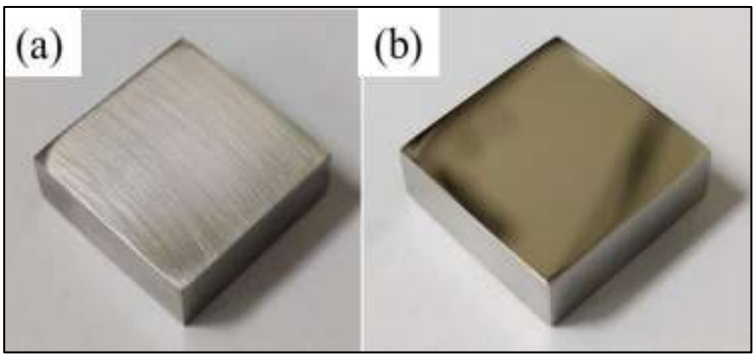

Fig. 3: Surface finish of specimens, (a) 1000 grit and (b) 1 micron

2.2. Pitting Corrosion Test

This work encompassed the implementation of two distinct pitting corrosion tests. Experimental Test No.1, which adhered to ASTM G48 Method A, involved a ferric chloride pitting test aimed at determining the corrosion rate of the test specimens within a chloride ion environment. Meanwhile, Experimental Test No.2, based on ASTM G48 Method E, constituted a critical pitting temperature test for stainless steel, serving to ascertain the critical pitting temperature of the test specimens and investigate pitting corrosion across various temperature ranges.

For Experimental Test No.1, the test solution was prepared by combining 540 mL of reverse osmosis (RO) water with 60 grams of ferric chloride powder. On the other hand, the test solution for Experimental Test No.2 was formulated by blending 600 mL of RO water, 68.72 grams of ferric chloride powder, and 16 mL of 37% concentrated hydrochloric acid. Following the preparation of the test solution, it was allowed to stabilise in a fume cupboard for a duration of 24 hours. Once the desired temperature was attained, the test solution underwent filtration using a grade 1 filter paper and a filter funnel. Before immersing the test specimen, its dimensions were measured, and its weight determined using a precision electronic balance with an accuracy of 0.001 grams. The test specimen was subsequently placed into a glass cradle, as depicted in Figure 4, and fully submerged in the test solution, as illustrated in Figure 5, for durations of 24 hours and 72 hours, respectively, for Experimental Test No.2 and Experimental Test No.1.

Experimental Test No.1 was conducted at a controlled room temperature of 27±2°C, while the temperature for Experimental Test No.2 was initially set at room temperature and progressively reduced by 5°C for each subsequent test until a temperature was reached at which pitting corrosion was no longer observed on the test specimen. After Experimental Test No.2, the corrosion pit depth on the surface of the specimen was measured with a surface profilometer (Mahr, model: MarSurf M 400C, Germany).

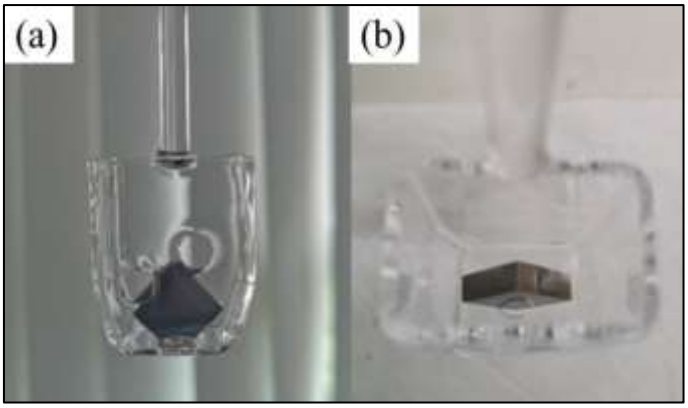

Fig. 4: Placement of specimen sample in glass cradle, (a) front view and (b) top view

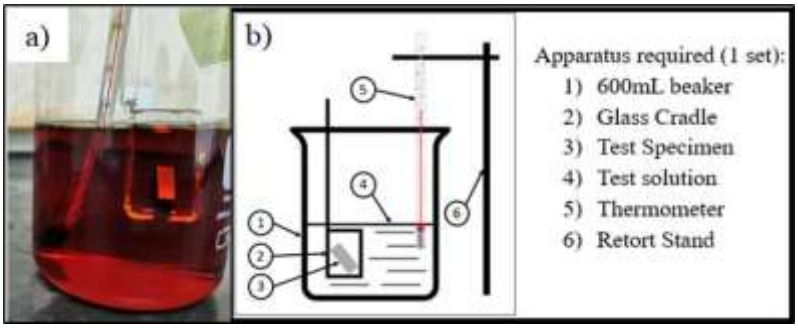

Fig. 5: (a) Photograph and (b) schematic diagram of experimental setup

2.3. Microstructural Analysis

Microstructural analysis was conducted using a metallurgical microscope (Meiji, Model: MT7100, Japan). Prior to etching the surface of the specimen samples to reveal the microstructure, it was necessary to polish the surface until achieving a 1-micron mirror finish, thereby eliminating all surface scratches. The polished test specimen surface was then subjected to etching using 37% concentrated hydrochloric acid for 5-minutes. The etched test specimens were observed and captured under the microscope to examine the microstructure. Grain size measurements were obtained from the microstructural images of each 316L stainless steel specimen. This involved drawing a line across the area with the highest number of grains and dividing the measured length by the total number of grains intersecting the line to determine the average grain size in microns.

2.4. Hardness Test

The hardness of the test specimen was measured using a Vickers hardness tester (Wilson Wolpert, Model: 450SVA, Germany). To ensure representative results, a total of five indentation measurements were taken on the surface (X-Y plane) of each test specimen, and the average hardness value was calculated. For 316L LPBF, 316L WAAM, 316L MBJ and 316L Wrought specimens, a 50 kgf load was applied to create an indentation, as illustrated in Figure 6.

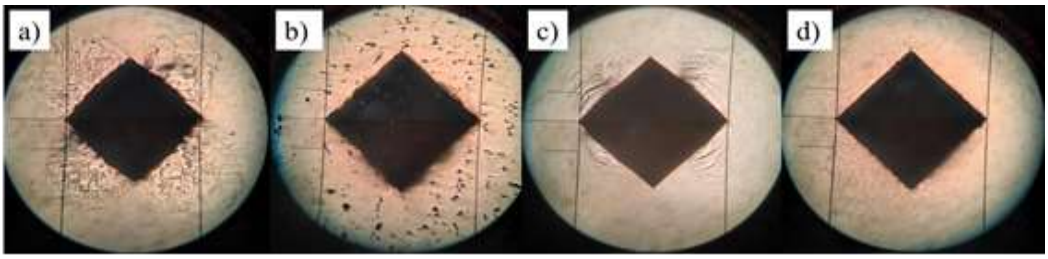

Fig. 6: Diamond shape indentation on sample surface of (a) 316L LPBF, (b) 316L MBJ, (c) 316L WAAM, and (d) 316L Wrought.

3. RESULTS AND DISCUSSION

3.1. Pitting Corrosion Results

Figure 7 presents the average corrosion rate of the different specimen samples in ascending order. Among the tested 316L stainless steel specimens, 316L LPBF exhibits the lowest corrosion rate of 6.87 mm per year. It is followed by 316L WAAM with a corrosion rate of 18.02 mm per year, 316L Wrought with a corrosion rate of 21.72 mm per year, and 316L MBJ, which shows the highest corrosion rate among all the specimens, at 46.30 mm per year.

Figure 8 illustrates the corrosion characteristics observed in various specimens of 316L stainless steel. The pitting corrosion observed in the 316L LPBF specimen exhibits a vertical grain attack pattern in which the printing pattern of the LPBF process is exposed due to different corrosion rate at the melt pool boundaries. The corrosion behavior of the 316L MBJ specimen resembles that of subsurface corrosion, with depressions forming on top of the material removal. In the case of the 316L WAAM specimen, pitting corrosion manifests as a shallow and wide corrosion shape on its surface. Lastly, the corrosion characteristic observed in the 316L Wrought specimen shows a horizontal grain attack. These visual observations can be further corroborated with microstructure analysis of the pit to unequivocally discern the mechanism of pit formation.

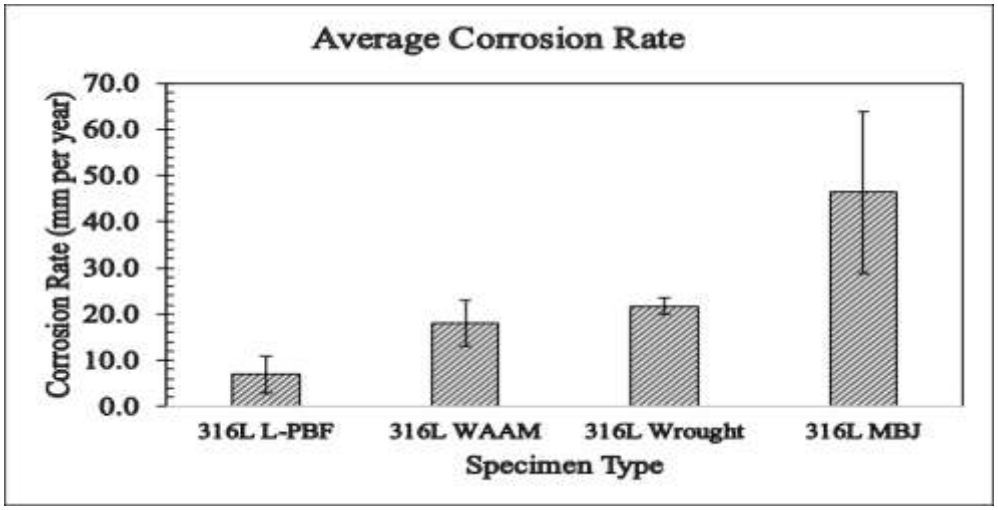

Fig. 7: Average corrosion rate of 316L Stainless Steels manufactured by different additive manufacturing methods (LPBF, WAAM, MBJ) compared to conventional method.

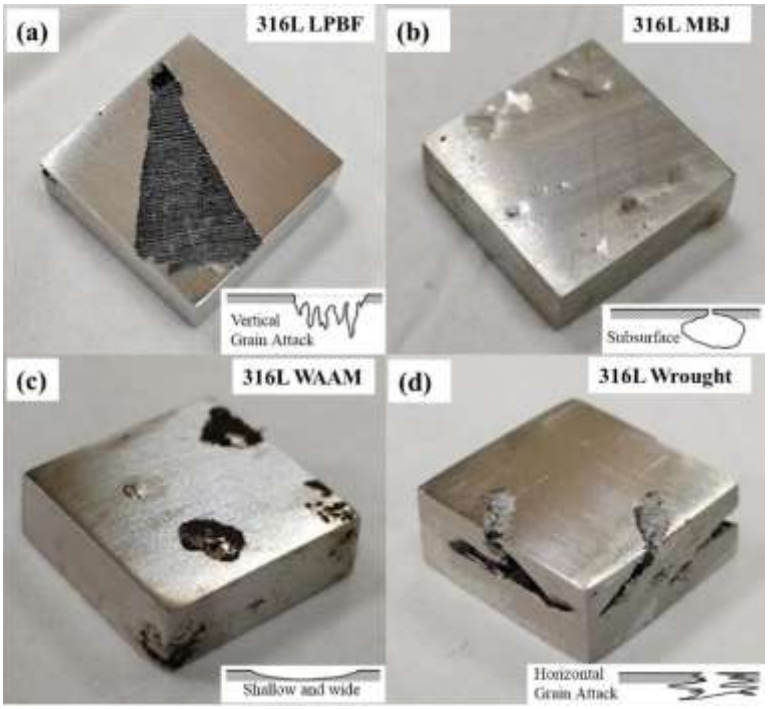

Fig. 8: 316L stainless steel corrosion characteristic of (a) LPBF, (b) MBJ, (c) WAAM, and (d) Wrought

The results of the study revealed notable variations in the pitting corrosion resistance performance among the tested specimen samples. Specifically, 316L stainless steel produced through the Laser Powder Bed Fusion (LPBF) additive manufacturing method exhibited the highest level of pitting corrosion resistance.

This was evidenced by its remarkably lower average corrosion rate and significantly higher critical pitting temperature. In contrast, the pitting corrosion resistance of 316L stainless steel fabricated via Metal Binder Jetting (MBJ) additive manufacturing method was found to be the weakest among all the tested samples.

Comparatively, 316L stainless steel manufactured through the Wire Arc Additive Manufacturing (WAAM) method displayed improved pitting corrosion resistance performance when compared to the traditionally hot-rolled 316L stainless steel (referred to as 316L wrought). However, it is important to note that even though the WAAM method showcased better pitting corrosion performance than the hot rolling method, it still fell short in terms of the pitting corrosion resistance achieved by the 316L LPBF specimen.

3.2. Critical Pitting Temperature

Table 1 presents the critical pitting temperature (CPT) values for the various specimen samples. The 316L LPBF specimen demonstrates a CPT range of 20 °C – 25 °C on the X-Y plane surface, while the Y-Z plane surface exhibits a CPT range of 15 °C – 20 °C. Conversely, the 316L MBJ specimen displays a CPT range of 10 °C – 15 °C on both the X-Y plane and Y-Z plane surfaces. In the case of the 316L WAAM specimen, the X-Y plane surface exhibits a CPT range of 15 °C – 20 °C, whereas the Y-Z plane surface demonstrates a CPT range of 10 °C – 15 °C. Notably, for the 316L Wrought specimen, a CPT range of 15 °C – 20 °C is observed on the X-Y plane surface. However, due to the persistence of pitting corrosion at the lowest tested temperature, the CPT for the Y-Z plane surface of 316L Wrought could not be determined.

Table 1: Test results for critical pitting temperature

Sample	Surface	Critical Pitting Temperature (±2.5°C)
316L LPBF	X-Y Plane	22.5
	Y-Z Plane	17.5
316L MBJ	X-Y Plane	12.5
	Y-Z Plane	12.5
316L WAAM	X-Y Plane	17.5
	Y-Z Plane	12.5
316L Wrought	X-Y Plane	17.5
	Y-Z Plane	N/A

Figures 9 to 12 display the corrosion pit cross-sectional profile and its depth (Pt) of 316L LPBF, 316L MBJ, 316L WAAM, and 316L Wrought specimens, respectively, for both the X-Y plane and Y-Z plane surfaces. The anisotropy between the X-Y and Y-Z planes on the critical pitting temperature is evident in LPBF and WAAM samples can be correlated to the layer-by-layer nature of both manufacturing processes. Columnar grains aligned to the build direction (Z) are commonly reported for those processes. Conversely, MBJ which is a sintering-based process presents a homogenous structure leading to similar corrosion susceptibility for both planes examined.

The profile depth measurements were conducted on the surface corrosion pits of the specimen samples to assess their respective depths. According to the ASTM G48 test standard guideline, a corrosion pit is considered significant if its depth exceeds 25 µm. All profile depth (Pt) measurements depicted in Figures 9 to 12 exhibit corrosion pits that surpass the 25-µm threshold for the corresponding test temperature.

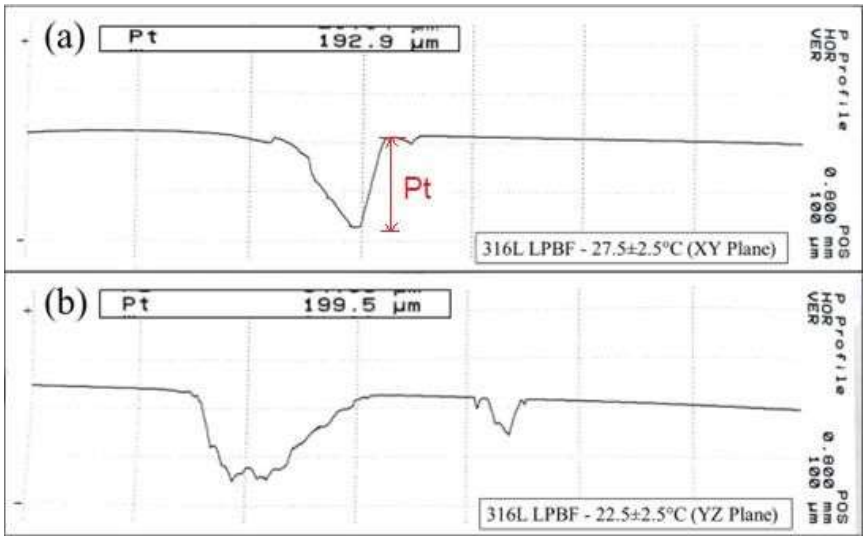

Fig. 9: Corrosion pit cross-sectional profiles of 316L LPBF on (a) X-Y and (b) Y-Z planes

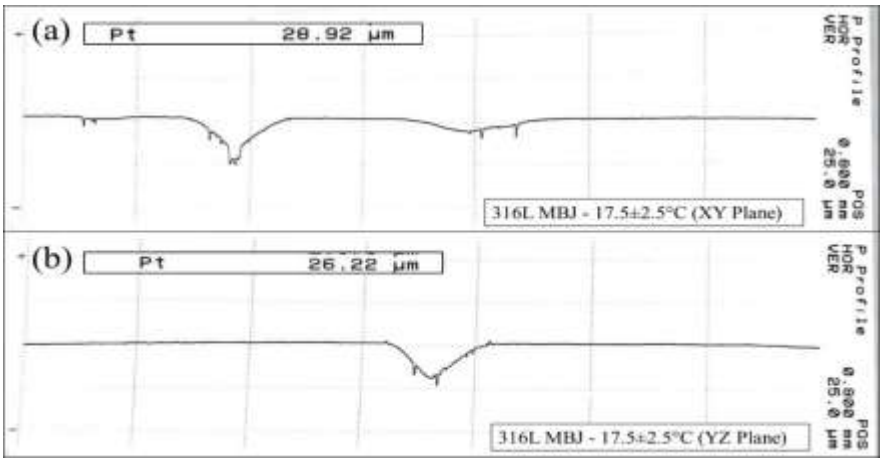

Fig. 10: Corrosion pit cross-sectional profiles of 316L MBJ on (a) X-Y and (b) Y-Z planes

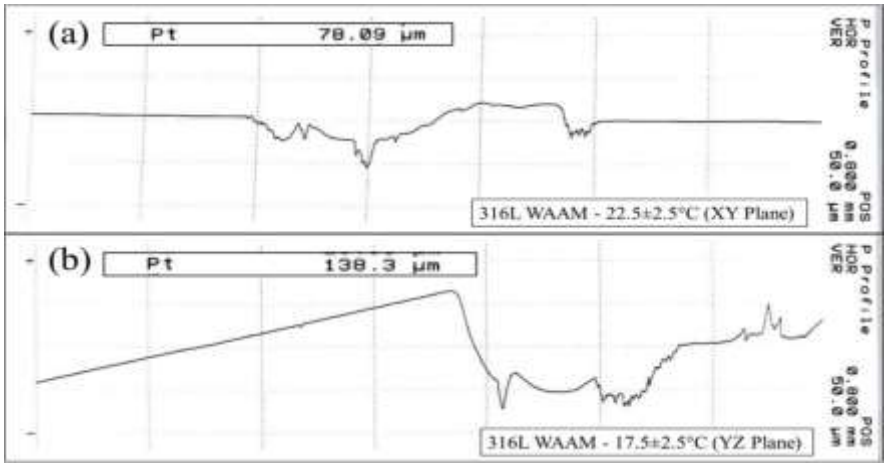

Fig. 11: Corrosion pit cross-sectional profiles of 316L WAAM on (a) X-Y and (b) Y-Z planes

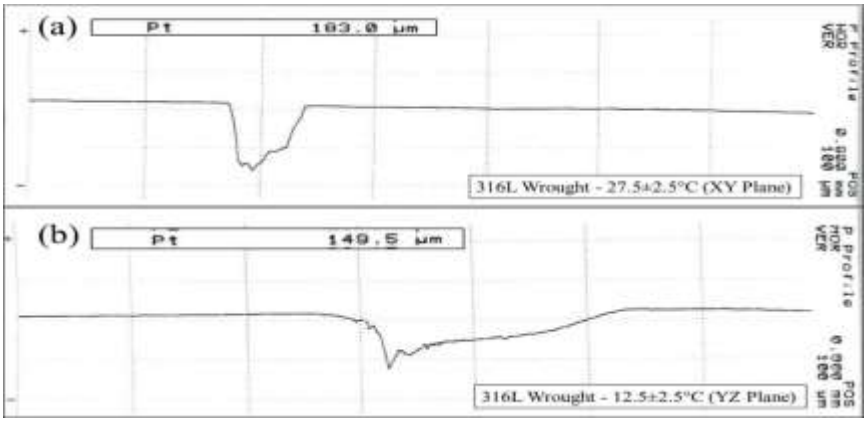

Fig. 12: Corrosion pit cross-sectional profile of 316L Wrought on (a) X-Y and (b) Y-Z planes

3.3. Microstructure Analysis

Figure 13 depicts the measurement of grain size for each of the 316L stainless steel specimen samples. The grain size analysis for the 316L LPBF sample was conducted at a magnification of 50x due to its smaller grain size. Conversely, the grain size measurements for 316L MBJ, 316L WAAM, and 316L Wrought

were performed at a magnification of 20×.

Table 2 provides the average grain size measurements for each specimen sample. The 316L LPBF stainless steel specimen exhibited the smallest average grain size, measuring 8 μm. Following that, the average grain size for 316L WAAM was determined to be 16.83 μm, while 316L Wrought displayed an average grain size of 19.79 μm. Lastly, the 316L MBJ stainless steel specimen exhibited the largest average grain size, measuring 33.65 μm.

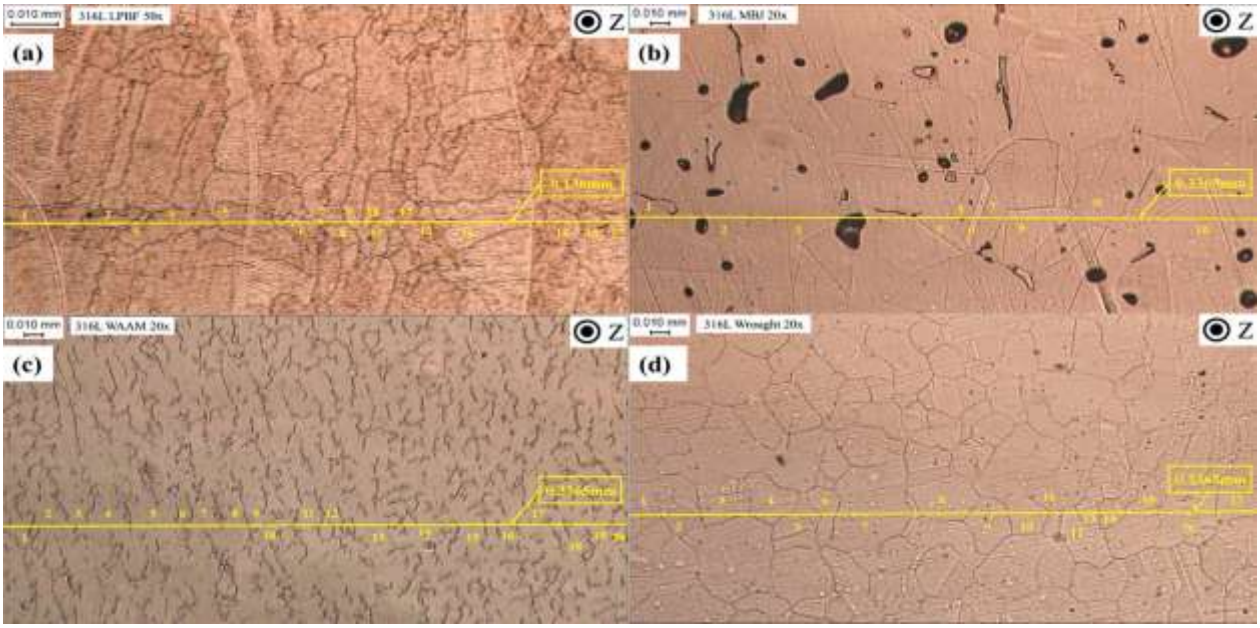

Fig. 13: Grain size measurement for (a) 316L LPBF (50×), (b) 316L MBJ (20×), (c) 316L WAAM (20×), (d) 316L Wrought (20×)

Table 2: Average grain size measurement

Specimen Type	Average Grain Size (μm)
316L LPBF	8.00
316L MBJ	33.65
316L WAAM	16.83
316L Wrought	19.79

In Figure 14, a noteworthy correlation between the average grain size and average corrosion rate is illustrated. The data indicates that specimen samples with larger grain sizes tend to display higher average corrosion rates. This suggests an inverse relationship between average grain size and average corrosion rate within the tested samples.

The grain size of the specimen is another significant factor that influences pitting corrosion resistance. The findings demonstrate that specimens with larger grain sizes, such as the 316L MBJ specimen, exhibit higher corrosion rates, refer to Figure 14. In contrast, specimens with smaller grain sizes, such as the 316L LPBF specimen, display lower corrosion rates. This correlation can be explained by the impact of grain boundaries on the material's electrochemical behaviour.

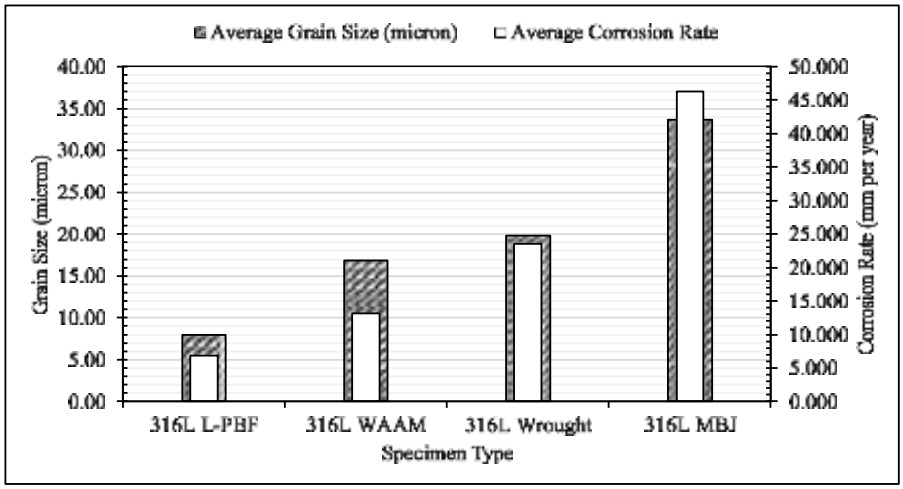

Fig. 14: Average grain size and average corrosion rate comparison for 316L stainless steel manufactured by different additive manufacturing (AM) methods and a hot rolling method.

A smaller grain size leads to a higher density of grain boundaries per unit area and volume of the material. Grain boundaries possess distinct electrochemical properties, making them more susceptible to corrosion attack. However, it has also been shown via electrochemical characterization that a more compact, stable and less defective native oxide is achieved with a finer microstructure which would explain the low corrosion susceptibility of L-PBF [14]. Also, comparing the behaviour of similar grain size L-PBF and wrought materials, it has been shown that the process-induced chemistry of the inclusions could play a strong role in influencing the pitting resistance [15]. Therefore, further research on the exact grain boundary composition is needed to fully understand the correlation observed in this study.

3.3. Vickers Hardness Results

Table 3 presents the results of the Vickers hardness tests conducted on the different specimen samples. Among them, the 316L LPBF stainless steel specimen sample exhibited the highest surface hardness, recording a Vickers hardness value of 232.12. Following closely is the 316L WAAM specimen with a Vickers hardness value of 197, while the 316L Wrought specimen displayed a Vickers hardness value of 174.78. Conversely, the 316L MBJ specimen showcased the lowest surface hardness, measuring a Vickers hardness value of 106.6.

Table 3: Vickers hardness test results for 316L LPBF, 316L MBJ, 316L WAAM, and 316L Wronght

Type	Average Vickers Hardness (HV_{50kgf})
316L LPBF	232.12
316L MBJ	106.60
316L WAAM	197.00
316L Wrought	174.78

Figure 15 illustrates a discernible correlation between the surface hardness and the corrosion rate of the specimen samples. Notably, the specimens with lower surface hardness exhibited higher corrosion rates. This observation suggests an inverse relationship between surface hardness and corrosion rate within the tested samples. A high hardness is generally associated with small grain size. Therefore, the relationship between corrosion susceptibility and hardness can be interpreted in conjunction with the grain size as seen in the previous section.

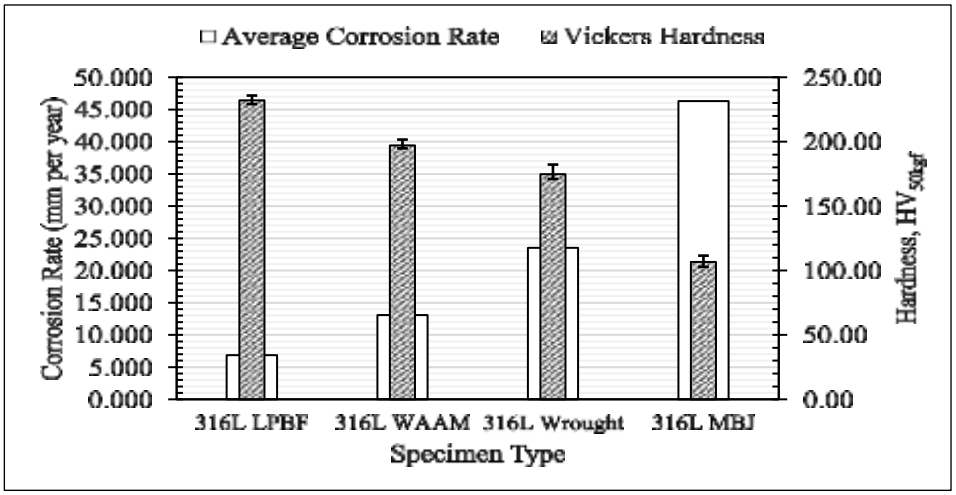

Fig. 15: Vickers hardness and average corrosion rate comparison for 316L stainless steel manufactured by different AM Methods and hot rolling method.

CONCLUSIONS

In summary, the findings of this study indicate that among the tested specimens, 316L stainless steel produced through the Laser-Powder Bed Fusion (LPBF) additive manufacturing (AM) method exhibited superior resistance to pitting corrosion. This was evidenced by its notably lower pitting corrosion rate and higher critical pitting temperature. Following 316L LPBF, the pitting corrosion resistance of 316L stainless steel manufactured via the Wire Arc Additive Manufacturing (WAAM) AM method ranked second. 316L stainless steel produced through the hot rolling method (referred to as 316L Wrought) and the Metal Binder Jetting (MBJ) AM method demonstrated comparatively lower pitting corrosion resistance.

Moreover, the investigation revealed that the microstructural characteristics and hardness of the specimens, as influenced by the manufacturing method, significantly influenced their pitting corrosion resistance. Microstructure analysis revealed that specimens with finer grain size exhibited enhanced resistance to pitting corrosion. Additionally, specimens with higher hardness exhibited improved pitting corrosion resistance.

It is expected that porosity rates will influence the susceptibility of the material to corrosion as the pores act as corrosion initiation sites. In this case, materials obtained with sintered-based processes such as MBJ would offer

the lowest resistance to corrosion and would be in agreement with the present study.

In conclusion, the results underscore the critical role of microstructure in determining the pitting corrosion resistance of 316L stainless steel specimens fabricated through different manufacturing methods.

ACKNOWLEDGEMENTS

The authors gratefully acknowledge Cetim - Matcor (Singapore) for the technical and financial support rendered. Special thanks to the Faculty of Engineering and Technology of Multimedia University for their support in allowing this research to be carried out.

REFERENCES

[1] U. M. Dilberoglu, B. Gharehpapagh, U. Yaman, and M. Dolen, 'The Role of Additive Manufacturing in the Era of Industry 4.0', Procedia Manuf., vol. 11, pp. 545–554, Jan. 2017, doi: 10.1016/j.promfg.2017.07.148.

[2] B. Blakey-Milner et al., 'Metal additive manufacturing in aerospace: A review', Mater. Des., vol. 209, p. 110008, Nov. 2021, doi: 10.1016/j.matdes.2021.110008.

[3] W. Jamróz, J. Szafraniec, M. Kurek, and R. Jachowicz, '3D Printing in Pharmaceutical and Medical Applications – Recent Achievements and Challenges', Pharm. Res., vol. 35, no. 9, p. 176, Jul. 2018, doi: 10.1007/s11095-018-2454-x.

[4] L. Gardner, P. Kyvelou, G. Herbert, and C. Buchanan, 'Testing and initial verification of the world's first metal 3D printed bridge', J. Constr. Steel Res., vol. 172, p. 106233, Sep. 2020, doi: 10.1016/j.jcsr.2020.106233.

[5] M. Orquéra, S. Campocasso, and D. Millet, 'Design for Additive Manufacturing Method for a Mechanical System Downsizing', Procedia CIRP, vol. 60, pp. 223–228, Jan. 2017, doi: 10.1016/j.procir.2017.02.011.

[6] T. D. Ngo, A. Kashani, G. Imbalzano, K. T. Q. Nguyen, and D. Hui, 'Additive manufacturing (3D printing): A review of materials, methods, applications and challenges', Compos. Part B Eng., vol. 143, pp. 172–196, Jun. 2018, doi: 10.1016/j.compositesb.2018.02.012.

[7] W. E. Frazier, 'Metal Additive Manufacturing: A Review', J. Mater. Eng. Perform., vol. 23, no. 6, pp. 1917– 1928, Jun. 2014, doi: 10.1007/s11665-014-0958-z.

[8] Medina Collana , J. T. ., Hurtado, D. G. ., Ramirez, D. M. ., Gonzales , J. P. S. ., Jimeenz, S. R. ., Huamani , J. A. R. ., Tasso , U. H. ., & Llanos, S. A. V. . (2023). Hydrodynamic Cavitation as Pretreatment for Removal of Hardness From Reverse Osmosis Reject Water. International Journal of Membrane Science and Technology, 10(2), 288-301. https://doi.org/10.15379/ijmst.v10i2.1198

[9] G. Sander et al., 'Corrosion of Additively Manufactured Alloys: A Review', Corrosion, vol. 74, no. 12, pp. 1318–1350, Oct. 2018, doi: 10.5006/2926.

[10] D. Nakhaie, A. Imani, M. Autret, R. F. Schaller, and E. Asselin, 'Critical pitting temperature of selective laser melted 316L stainless steel: A mechanistic approach', Corros. Sci., vol. 185, p. 109302, Jun. 2021, doi: 10.1016/j.corsci.2021.109302.

[11] R. Davalos Monteiro, J. van de Wetering, B. Krawczyk, and D. L. Engelberg, 'Corrosion Behaviour of Type 316L Stainless Steel in Hot Caustic Aqueous Environments', Met. Mater. Int., vol. 26, no. 5, pp. 630–640, May 2020, doi: 10.1007/s12540-019-00403-2.

[12] T. Kumaran, B. Kannan, M. UTHAYAKUMAR, and P. Padmanabhan, 'Corrosion Studies on Stainless Steel 316 and their Prevention – A Review', INCAS Bull., vol. 13, pp. 245–251, Sep. 2021, doi: 10.13111/2066- 8201.2021.13.3.21.

[13] Jam, F., Donia, M., Raja, U., & Ling, C. (2017). A time-lagged study on the moderating role of overall satisfaction in perceived politics: Job outcomes relationships. Journal of Management & Organization, 23(3), 321-336. doi:10.1017/jmo.2016.13

[14] H. D. Carlton, A. Haboub, G. F. Gallegos, D. Y. Parkinson, and A. A. MacDowell, 'Damage evolution and failure mechanisms in additively manufactured stainless steel', Mater. Sci. Eng. A, vol. 651, pp. 406–414, Jan. 2016, doi: 10.1016/j.msea.2015.10.073.

[15] K. Tantratian, H. Yan, and L. Chen, 'Predicting pitting corrosion behavior in additive manufacturing: electro- chemo-mechanical phase-field model', Comput. Mater. Sci., vol. 213, p. 111640, Oct. 2022, doi: 10.1016/j.commatsci.2022.111640.

[16] R. I. Revilla et al., 'Microstructure and corrosion behavior of 316L stainless steel prepared using different additive manufacturing methods: A comparative study bringing insights into the impact of microstructure on their passivity', Corros. Sci., vol. 176, p. 108914, Nov. 2020, doi: 10.1016/j.corsci.2020.108914.

[17] Q. Chao et al., 'On the enhanced corrosion resistance of a selective laser melted austenitic stainless steel', Scr. Mater., vol. 141, pp. 94–98, Dec. 2017, doi: 10.1016/j.scriptamat.2017.07.037.

DOI: https://doi.org/10.15379/ijmst.v10i1.1814